Swelling behavior of compacted bentonite with the presence of rock fracture

Xia Bian, Yu Jun Cui, Ling-Ling Zeng, Xiao-Zhao Li

Swelling behavior of compacted bentonite with the presence of rock fracture

Xia Bian[a,b,c], Yu-Jun Cui[c], Ling-ling Zeng[d], Xiao-Zhao Li[b]

a: Key Laboratory of Ministry of Education for Geomechanics and Embankment Engineering, Hohai University, Nanjing 210098, China
b: Institute for Underground Space and Geoenvironment, School of Earth Sciences and Engineering Nanjing University, Nanjing, 210046, China
c: Ecole des Ponts ParisTech, Laboratoire Navier/CERMES, 6 et 8 Av. B. Pascal, F-77455 Marne-la-Vallée cedex 2, France
d: Institute of Geotechnical Engineering, College of Civil Engineering, Fuzhou University, Fuzhou 350108, China.

Corresponding Author:
Prof. Yu-Jun Cui
Laboratoire Navier/CERMES
Ecole des Ponts ParisTech
6 et 8 Av. B. Pascal, F-77455 Marne-la-Vallée cedex 2, France
Email: yu-jun.cui@enpc.fr

Abstract

In this study, the influence of rock fracture on the swelling behavior of compacted bentonite was investigated experimentally with bentonite compacted inside a hollow cylinder of fractured Beishan granite from China. During the test, hydration was allowed by letting water flowing into the compacted bentonite from the base plate, and air being expelled from the top plate. Along the sample, swelling pressure and relative humidity were monitored at different positions. Results showed that the presence of rock fracture significantly changed the hydration process of compacted bentonite. The evolutions of swelling pressure were directly related to the relative position to the rock fracture. At the same height, for the position closer to the rock fracture, a larger decrease in local dry density occurred, resulting in a larger loss in swelling pressure. This suggests that in field conditions of radioactive waste repository involving bentonite and rock, local filling of rock fracture by bentonite may occur, and the resulted bentonite swelling pressure decrease must be accounted for in the safety evaluation of the whole storage system.

Keywords: Radioactive waste disposal; rock fracture; bentonite; swelling pressure, relative humidity

1. Introduction

In the concept of deep geological repository for high level radioactive waste (HLW), compacted bentonites were often considered as potential material of engineered barrier, placed between the natural barrier (host rock) and the canister. After emplacement, compacted bentonites were expected to swell in contact with water, providing a required swelling pressure to fulfill the sealing functions, and isolating the HLW from the biosphere (Gens et al., 2002; Sun et al., 2009; Villar et al., 2005; Wang et al., 2013a, b).

In the repository, engineered barriers often consisted of compacted bentonite bricks. When the bricks were used to seal the repository, technological voids were left between the bricks or between the bricks, the canister and the host rock. Moreover, it is commonly admitted that there are natural fractures and fractures caused by excavation in the host rocks (Villar et al., 2005, Marshall et al., 2008; Armand et al., 2014). When water infiltrated from the host rock, the compacted bentonites swelled, filling up these macro-voids (technological voids and rock fractures) and further swelling pressure will develop under constrained space condition (Wang et al., 2013a, c, Bian et la., 2018). Hence, the presence of these macro-voids can significantly affect the hydro-mechanical behavior of the compacted bentonite, which may in turn influence the long-term performance of the sealing function of the repository (Villar and Lloret, 2008; Gens et al., 2011).

To investigate the influence of macro-voids on the hydro-mechanical behavior of compacted bentonites, oedometer tests with technological voids and small-scale mock-up tests with initial voids were carried out in the laboratory. Wang et al. (2012, 2013 c, 2014) and Saba et al.

(2014a) performed a series of oedometer tests with different sample diameters to simulate the technological voids. Their results confirmed that the presence of technological voids led to the decrease in global dry density, which eventually resulted in the variations of swelling pressure and permeability. The evolution of swelling behavior with the presence of initial voids was clearly related to the changes in microstructure during hydration (Romero et al., 1999, 2011; Wang et al., 2013a, 2014; Saba et al., 2014a). Several researchers also conducted small-scale mock-up tests to study the hydro-mechanical behavior of compacted bentonite with initial voids (Wang et al., 2013b; Saba et al., 2014b, 2016). In these works, certain axial movements of top plate were allowed to simulate the initial voids, and the relative humidity and swelling pressure along the sample were monitored during hydration. Bian et al. (2018) performed a series of infiltration tests on compacted bentonite with initial voids, and suggested that the initial voids resulted in heterogeneous dry density of bentonite and its evolution was correlated to the microstructure change. However, the above-mentioned laboratory tests involved cells made of stainless steel, which are not representative of the real condition in the repository with rock/compacted bentonite interface.

Regarding the rock/compacted bentonite interface, Baik et al. (2007) performed a mock-up test on a granite core with an artificial fracture and a compacted bentonite block to study the erosion of bentonite particles at the fracture. Ye et al. (2012) used the granite from Beishan (the potential site for deep geological repository in China) as the cell in an infiltration test to investigate the evolution of swelling pressure and hydraulic behavior of compacted bentonite. Chen et al. (2014) conducted a series of tests to study the hydraulic behavior of Boom clay/compacted bentonite interface. However, few attention has been paid on the influence of

rock fracture on the swelling behavior of compacted bentonite. To the authors' knowledge, there was no mock-up test performed on the rock sample with natural fracture to study its effect on the swelling behavior of compacted bentonite.

In this study, an experimental device was developed, allowing the influence of rock fracture on the swelling behavior of compacted bentonite to be investigated. The device consisted of a hollow rock column with the presence of natural fracture and the bentonite compacted inside. Along the sample, swelling pressure and relative humidity sensors were installed at various positions. The obtained results allowed further evaluation on the influence of rock fracture on the swelling behavior of compacted bentonite.

2. Experimental Setup

The basic scheme of the infiltration test is presented in Fig. 1. The experimental setup consisted of three parts: (i) the main body which was made of a hollow fractured Beishan granite cylinder and the compacted bentonite inside; (ii) the water supply system for water infiltration into the bentonite; and (iii) the monitoring system that compassed all the sensors (pressure sensors and relative humidity sensors) and the data logger linked to a computer.

The hollow rock cylinder consisted of two parts of granite samples with a natural fracture. As shown in Fig. 2, when the two parts of granite were put together, a well-defined natural facture was formed with a width ranging from 0.1 to 5.6 mm. The height of the assembled rock cylinder was 282 mm. The inner diameter of the cylinder ranged from 82 to 84 mm (average diameter of 82.5 mm). Note that the hollow part was not centered in the rock sample,

with the wall thickness of rock varying from 32 to 58 mm, due to the fact that the hollow cylinder granite was directly drilled from the Beishan site and it was hard task to handle the drilling tools in the field conditions. The hollow rock cylinder was placed on a stainless steel plate (base plate) with a porous stone on it, where the interface between the rock and the base plate was sealed by elastic rubber to prevent water leakage. After the sample was compacted inside the rock cylinder, a porous stone and a stainless steel plate were installed on its top. Six screw arbors were used to fix the rock cylinder vertically, while two pieces of stainless steel bars with screws were attached to the top and base plates to prevent the radial movements. In addition, the rock was covered by a rubber membrane to prevent water evaporation though the rock.

For the infiltration test, the water supply system was operated through a water inlet in the base plate, which was connected to a graduated water tank hanged at about 1 m higher than the base (corresponding to 10 kPa injection pressure). The air outlet was located at the top plate, and attached to a plastic tube, that was immersed in water in order to prevent water evaporation. During the infiltration test, the volume of water infiltrated into the compacted bentonite was monitored by recording the change of water level in the water tank.

There were five total pressure sensors and ten relative humidity sensors installed to monitor the swelling behavior of compacted bentonite with the presence of rock fracture, as shown in Fig. 3. Miniature pressure sensors protected by a stainless steel shell were installed through the ports in the wall of the rock cylinder. Fig. 3(a) shows that five pressure sensors were installed along three different sections. Along section 6#, three pressure sensors were placed

131 at 120 mm, 180 mm and 240 mm, namely PS120I, PS180F and PS240, respectively. In
132 addition, PS120F was installed at 120 mm along section 1# and PS180N was installed at 180
133 mm along section 3#. Hence, there were two sensors installed at 120 mm and 180 mm along
134 different sections, with different relative distances to the fracture. As shown in Fig. 3(b), the
135 vertical distances to the fracture for sensor PS120F and PS120I were 10 mm and 80 mm,
136 respectively. Sensors PS180N and PS180F were situated at about 12 mm and 20 mm below
137 the fracture, respectively.
138 Fig. 3(c) depicts that ten relative humidity (RH) sensors were installed every 60 mm along the
139 sample (60, 120, 180 and 240 mm). To avoid the disturbance of rock cylinder, all the RH
140 sensors were directly placed inside the compacted bentonite at the predetermined height. At
141 each height, one RH sensor was installed at the center of the sample. For the height of 120,
142 180 and 240 mm, the two other RH sensors were installed near the interface between rock and
143 bentonite. A digital displacement transducer was installed at the top plate to monitor the
144 vertical movement of the system during the infiltration test.
145

146 **3. Materials and Test Procedure**

147 The granite cylinder was obtained from Gansu Beishan, China, which has been considered as
148 a potential host rock for the deep geological repository in the Chinese HLW disposal program.
149 The granite can be classified as a fine-grained granodiorite with low porosity (0.29–0.32%).
150 The average grain density is 2.71 Mg/m^3 and the natural density is about 2.64 Mg/m^3. The
151 main composition of Beishan granite consisted of approximately 52% plagioclase, 17% quartz,
152 15% alkalifeldspar, 12% biotite, 3% albite, and <1% myrmekite (Chen et al., 2014). The
153 elastic modulus of Beishan granite is about 60 GPa and the permeability of Beishan granite is

154 approximately 10^{-11}~10^{-13} m/s (Wang, 2010; Chen et al., 2014).

155 The MX80 bentonite studied was from Wyoming, USA, with a montmorillonite content of
156 80%. It is one of the reference materials proposed as the engineering barrier in deep nuclear
157 disposal programs. The liquid limit and plastic limit of this bentonite are 575% and 53%,
158 respectively. The unit mass of the solid particles is 2.77 Mg/m^3. The cation exchange capacity
159 (CEC) is 76 meq/100 g (83% of Na) (Wang et al., 2013c). The bentonite powder has an initial
160 water content of 10.6% in ambient laboratory condition.

161

162 The MX80 bentonite was statically compacted inside the hollow rock cylinder. The
163 dimensions of the compacted bentonite are 272 mm in height, with an average diameter of
164 82.5 mm corresponding to the inner diameter of rock cylinder. The sample was compacted in
165 13 layers to obtain a homogenous sample at a target dry density of 1.33 Mg/m^3. The detailed
166 compaction procedure is listed in Table 1. The obtained sample height was 272.2 mm and the
167 mean dry density obtained was 1.32 Mg/m^3, close to the target value. During compaction, the
168 holes for the pressure sensor were blocked using a screwing solid plugs with the same shape
169 of the pressure sensors. When the soil was compressed to a target height, the RH sensors were
170 placed on the predetermined position. Then, the subsequent layer of soil was used to cover
171 and fix the RH sensors, and compacted to the target height afterwards. Note that the wires of
172 upper four RH sensors were pulled out through the hole at the top plate, while the wires of
173 lower six RH sensors were extracted from the hole at 30 mm. The holes for wire-out were
174 sealed with the elastic rubber.

175

176 After compaction of the bentonite, the blocked hole was replaced by the pressure sensor. The

177 stainless steel shell with pressure sensor was first smeared by glue, and then plugged into the
178 ports on the rock wall. The positions of the sensors were adjusted to obtain an initial pressure
179 of about 20 kPa, ensuring the good contact between the sensors and the sample. When the
180 initial contact achieved, a filament tape was used to fix the position of the sensors.
181
182 After the whole system was assembled, a 24-hour period was waited to ensure the glue
183 sealing the rock and plate interface, and fixing the position of pressure sensors. Water
184 infiltration was then performed from the bottom of the compacted bentonite. The swelling
185 pressures at different heights were recorded during hydration as well as the relative humidity
186 measured through RH sensors. Meanwhile, the vertical displacement of the top plate was also
187 monitored by the displacement transducer. As shown in Fig. 4, the axial movement of top
188 plate increased rapidly with time and reached a peak value of 0.23 mm after about 7 days of
189 hydration, corresponding to 0.09% of the sample height which was negligible. Thereby, the
190 test can be regarded as in constant volume condition during hydration.
191
192 **4. Results**
193 Fig. 5 shows the evolutions of swelling pressure with time. The initial value of all five
194 pressure sensors varied from 11 to 24 kPa, which indicated the good contact between the
195 pressure sensors and the compacted bentonite. With water infiltration, a quick increase of
196 swelling pressure followed by stabilization was observed at different heights. A gradually
197 slight decrease in swelling pressure was identified from 6500 hours. This trend was in
198 agreement with the evolution of swelling pressure from the mock-up test by Saba et al. (2014).
199 As water migrated upwards from water inlet, the first quick increase stage recorded by the

sensors at different heights were quite different, with the highest increase rate at 120 mm. This increase rate gradually decreased from 180 mm to 240 mm. At the same height, the increase rate changed with the relative distance to rock fracture, with lower increase rate for the position closer to the fracture.

Note that, the evolution of swelling pressure at the same height was directly affected by the presence of rock fracture. For sensor PS120I, a sudden decrease in swelling pressure was observed after water infiltration until about 75 hours (see Fig. 5b). This sudden drop might relate to the experimental design as discussed in latter section. After the first 75 hours, the swelling pressure exhibited a quick linear increase up to 1200 hours. Afterwards, the swelling pressure slowly increased and reached a peak value of 196 kPa, followed by a slight decrease to a final value at about 157 kPa. At the same height but close to the fracture, the evolution of swelling pressure measured by sensor PS120F showed a similar pattern as that of sensor PS120I, except for the first sudden drop. However, the peak and final value of swelling pressure recorded by sensor PS120F were about 110 and 73.7 kPa, respectively, which were significant lower than that measured by PS120I. This difference can be attributed to the influence of rock fracture. At 180 mm, the swelling pressure increased at similar initial rate for sensor PS180N and PS180F up to 1400 hours, which was lower than that at 120 mm. After 1400 hours, the difference in swelling pressure between sensor PS180N and PS180F occurred and increased to about 42 kPa at 8300 hours. Again, this difference resulted from different distances of sensors from the rock fracture, that is: the position of sensor PS180N was about 8 mm closer to the fracture than that of sensor PS180F. Fig. 6 shows the relationship between peak and final swelling pressure and the distance to the fracture at 120 and 180 mm. It is clear that with the presence of rock fracture, the relative position to the fracture showed significant

effect on the peak and final swelling pressure. At 120 mm, the difference in distance to the fracture for sensor PS120F and PS120I was 70 mm, which led to a difference in swelling pressure of 86 kPa (peak value) and 83.3 kPa (final value). For the case at 180 mm, the differences in swelling pressure of 51 kPa (peak value) and 42 kPa (final value) were mainly due to the 8 mm difference in distance to the fracture between sensor PS180N and PS180F. It can also be observed that, greater relative distance to the fracture at the same height resulted in higher difference in swelling pressure.

During the test, the changes in relative humidity (RH) at different positions are presented in Fig. 7. The initial RH values were about 44±1%, corresponding to the initial water content of 10.6%. On the whole, the RH value increased with time after water was introduced (for sensors located in the center of the sample, as shown in Fig. 7a). At 60 mm, the RH value showed a decrease trend up to 70 hours, and increased rapidly to 99% at 200 hours. This sudden decrease in RH at lower position can explain the sudden decrease in swelling pressure mentioned previously. As shown in Fig. 7b, the RH value at 120 mm, 180mm and 240 mm started to increase after about 40 hours, 50 hours and 100 hours respectively, indicating the gradual migration of water from the water inlet upwards (from bottom to top). Similar observations have also been reported by Wang et al. (2013a) from the mock-up test on the compacted bentonite and sand mixture. Unlike the results reported by Wang et al. (2013a), the changes in relative humidity at different heights showed discontinues pattern with sudden increase followed by a plateau. This behavior is mainly due to the fact that the air in the porous stone and the water inlet tube did not been fully evacuated before the water injection. Hence, the trapped air bubble might result in the discontinues of water infiltration. This

behavior can be confirmed by the variation of recordings of sensors near the rock/bentonite interface as shown in Fig. 7c. As water infiltration continued, RH sensors located close to the bentonite/rock interface at heights of 120 mm, 180 mm and 240 mm showed a delay response in recording of relative humidity. Comparisons between Fig. 7(b) and 7(c) showed that at the same height, the detection times of sensors near the rock/bentonite interface were about dozens of times longer than that in the middle of the bentonite. At longer time, a sudden increase in relative humidity for sensors near the rock/bentonite interface was also observed. This phenomenon is thought to be due to that the air bubble was mainly distributed near bentonite/rock interface, resulting in difficulty of upward water migration from the positon close to bentonite/rock interface. However, water could move from the center of the sample to higher position (RH value rapidly increased with time recorded by sensor located in center of sample at different positions).

5. Discussion

The aim of the presented experimental test was to study the influence of rock fracture on the swelling behavior of compacted bentonite. Fig. 8 shows a photo of rock fracture after dismantling. The dash line depictes the rock inner wall, while the solid line represents the bentonite/rock interface after test. Sensor RH6 can be also observed in the figure. It appears clearly that after 349-day hydration, the bentonite/rock interface enlarged about 1-2 mm. This confirms the intrusion of bentonite into the rock fracture under the effect of swelling pressure of bentonite behind. Hence, it is logically to expect that the loss of swelling pressure with the presence of rock fracture (see Fig. 6) was mainly due to the decrease in local dry density in the vicinity of the fracture when certain amount of bentonite filling the fracture. This behavior

is consistent with the result of influence of technological void on the swelling behavior of compacted bentonite and sand mixture (Wang et al., 2012, 2013a, c). The presence of technological voids resulted in a decrease in global dry density and consequently led to a decrease in swelling pressure. As shown in Fig. 2, the height of the rock fracture across the sample is about 70 mm. If assumed that only the compacted bentonite within the perimeter of the fracture (the cylinder of 70 mm in height and 82.5 mm in diameter) were significantly influenced by the intrusion of bentonite into rock fracture, the local technological void defined by rock fracture can be calculated as:

$$tv\ (\%) = V_{\text{fracture}} / V_{\text{local compacted bentonite}} \quad (1)$$

where V_{fracture} = the volume of rock fracture (34 cm^3), $V_{\text{local compacted bentonite}}$ = the volume of compacted bentonite influenced by rock fracture (374 cm^3). Hence, the local technological void influenced by rock fracture is equal to approximately 9.1%.

Wang et al. (2012) proposed the relationship between the final bentonite dry density and the swelling pressure for MX80 bentonite as follows:

$$\sigma_s = \alpha \times \exp(\beta \rho_{dp}) \quad (2)$$

where σ_s is the swelling pressure, ρ_{dp} is the bentonite dry density, α and β are the soil constants, equal to 1.78×10^{-4} and 6.75, respectively for MX80 bentonite.

The peak values of swelling pressure for the five sensors ranged from 255 to 110 kPa. These results were compatible with the swelling pressure predicted by Eq. (2) for a mean value dry density of 1.20 Mg/m^3, which corresponded to the initial dry density 1.32 Mg/m^3 with about 10% of technological void. As shown in Fig. 3, sensor PS120I was far from the fracture (80 mm distance), while PS120F was located at a closest positon, with about 10 mm from the fracture. Hence, the difference between these two sensors could represent the effect of local

292 technological void caused by rock fracture. By back-calculating the final dry density using Eq.
293 (2) according to the two measured peak values of swelling pressure at 120 mm, it was found
294 that the difference in dry density was approximately 9.5%. This value is consistent with the
295 local technological void defined by the fracture geometry and the difference in swelling
296 pressure. Moreover, the difference in dry density at 180 mm identified by the measured values
297 for sensors PS180N and PS180F was about 3.5%. These results suggested that a higher
298 decrease in local dry density at a closer distance to fracture, after materials intruded into the
299 fracture, resulted in a larger loss of swelling pressure.
300
301 Regarding the sudden decrease of swelling pressure for sensor PS120I, it can be explained by
302 combining the results of swelling pressure sensors and RH sensors. As shown in Fig. 7, the
303 RH value at 60 mm decreased until about 70 hours. This decrease possibly resulted from the
304 experimental design where the connection wires of RH sensor at position lower than 180 mm
305 were pulled out of the sample through the hole located at 30 mm (as shown in Fig. 9).
306 Although the hole was sealed by the elastic rubber after the wire pulled out, some air can still
307 flow into the sample through the hole, which may lead to the first decrease in RH value at 60
308 mm after water injection. In addition, because there were lots of wires going through the hole
309 at 30 mm, this may result in local inhomogeneous distribution of soil around this area. After
310 water infiltration, the soil around the hole at 30 mm tended to swell and reorganize.
311 Meanwhile, air might go inside the sample through the hole at 30 mm. All these factors might
312 result in the local soil redistribution or local soil collapse around the area near 30 mm hole.
313 This, in turn, led to the decrease in swelling pressure of sensor PS120I along section 6# at the
314 beginning of the test. Fig. 10 shows a photo of sample at 60 mm after sample dismantled. It

315 can be observed that the converged wires of RH sensor around 60 mm along section 6#
316 significantly disturbed the soil around that positon. The sample at different sections were
317 taken and the dry density of after-infiltration sample at 60 mm were determined as shown in
318 Fig. 11. It is clear that the dry density of after-infiltration sample along section 6# (near 30
319 mm hole) was the lowest, which confirmed that the looser state of soil was caused by the
320 wires of RH sensors and explained the sudden decrease in swelling pressure for sensor
321 PS120I.
322
323 As expected, during the test, water was gradually absorbed by the compacted bentonite from
324 water inlet. Hence, the RH sensors gradually reacted from lower layer to upper layer. This is
325 similar to the variations of RH recording from the mock-up test reported by Wang et al.
326 (2013a). However, it should be pointed out that the changes in RH with time reported by
327 Wang et al. (2013a) seemed more smooth than that presented in this study. This is mainly due
328 to the fact that the air in porous stone and the connection tube were not fully expelled before
329 the test. As a result, the air bubbles were accumulated around the interface between rock and
330 compacted bentonite (the delay reaction of RH sensors near the rock/bentonite interface at the
331 beginning), which resulted in a discontinued pore channel within the compacted bentonite.
332 During the test, the water migration may be disrupted by this discontinued pore channel,
333 leading to the discontinued development of relative humidity observed.
334
335 The obtained results showed that the swelling behavior of compacted bentonite was directly
336 influenced by the presence of rock fracture, with a higher decrease in swelling pressure at a
337 closer position from the rock fracture. This behavior suggests that in the real repository, local

failure of compacted bentonite due to the presence of rock fracture may occur and it should be taken into account in the design of the engineering barrier. On the whole, the results from this test provide valuable data to qualitatively analyze the influence of rock fracture on the swelling behavior of compacted bentonite, which is in agreement with the existing data from infiltration tests with technological voids (Wang et al. 2013b, Saba et al., 2014b, 2016). This confirms the applicability of this experimental method and the experimental device developed.

6. Conclusions

An experimental device was developed for investigating the influence of rock fracture on the swelling behavior of compacted bentonite. An infiltration test was carried out using this experimental setup. It was observed that when water was infiltrated into the sample, water gradually migrated from bottom layer to top layer, with the relative humidity recorded by RH sensors progressively increased along the sample. This process corresponded to the gradual increase in swelling pressure, with a higher increase rate at a position closer to the water inlet. The presence of rock fracture showed significant influence on the development of swelling pressure. For a position closer to the rock fracture, a larger decrease in local dry density occurred, resulting in a larger decrease in swelling pressure. The results obtained from this experiment suggest that the local loss of swelling pressure of compacted bentonite may occur due to the local decrease in dry density of engineered barrier with the presence of rock fracture in deep geological repository.

Acknowledgements

The authors thank the China Postdoctoral Science Foundation (Grants No. 2016M600396, 2017T100355) and the Fundamental Research Funds for the Central Universities of China (Grant No. 2018B13514) for the financial support. They also acknowledge the support provided by the European Commission by the Marie Curie IRSES project GREAT - Geotechnical and geological Responses to climate change: Exchanging Approaches and Technologies on a world-wide scale (FP7-PEOPLE-2013-IRSES-612665).

References

Armand, G., Leveau, F., Nussbaum, C., de La Vaissiere, R., Noiret, A., Jaeggi, D., ... & Righini, C. (2014). Geometry and properties of the excavation-induced fractures at the Meuse/Haute-Marne URL drifts. Rock Mechanics and Rock Engineering, 47(1), 21-41.

Baik, M. H., Cho, W. J., & Hahn, P. S., 2007. Erosion of bentonite particles at the interface of a compacted bentonite and a fractured granite. Eng. Geol. 91(2), 229-239.

Bian, X., Cui, Y. J., Li, X. Z. Voids effect on the swelling behaviour of compacted bentonite. Géotechnique, online, https://doi.org/10.1680/jgeot.17.p.283.

Chen, L., Liu, J. F., Wang, C. P., Liu, J., Su, R., and Wang, J., 2014. Characterization of damage evolution in granite under compressive stress condition and its effect on permeability. Int. J. Rock. Mech. Min. Sci. 71, 340-349.

Chen, Y. G., Cui, Y. J., Tang, A. M., Wang, Q., and Ye, W. M., 2014. A preliminary study on hydraulic resistance of bentonite/host-rock seal interface. Géotechnique, 64 (12), 997-1002.

Marschall P, Trick T, Lanyon GW, Delay J, Shao H. Hydro-mechanical evolution of damaged zones around a microtunnel in a claystone formation of the Swiss Jura Mountains. In: Proceedings of the 42rd US rock Mechanics Symposium, SanFrancisco, 2008. ARMA08-193.

Gens, A., Guimaraes, L. D. N., Garcia-Molina, A., and Alonso, E. E., 2002. Factors controlling rock–clay buffer interaction in a radioactive waste repository. Eng. Geol. 64 (2), 297-308.

389 Gens, A., Vállejan, B., Sánchez, M., Imbert, C., Villar, M. V., and Van Geetl, M., 2011.
390 Hydromechanical behaviour of a heterogeneous compacted soil: experimental
391 observations and modelling. Géotechnique, 61 (5), 367-386.
392 Romero, E., Gens,A., Lloret,A.,1999.Waterpermeability,waterretention and microstructure of
393 unsaturated compacted Boom clay. Eng. Geol.54, 117–127.
394 Romero, E., Della Vecchia, G., Jommi, C., 2011. An insight into the water retention properties
395 of compacted clayey soils. Geotechnique 61 (4), 313–328.
396 Saba, S., Barnichon, J. D., Cui, Y. J., Tang, A. M., and Delage, P., 2014a. Microstructure and
397 anisotropic swelling behaviour of compacted bentonite/sand mixture. J. Rock Mech.
398 Geotech. Eng. 6 (2), 126-132.
399 Saba, S., Cui, Y. J., Tang, A. M., & Barnichon, J. D., 2014b. Investigation of the swelling
400 behaviour of compacted bentonite–sand mixture by mock-up tests. Can. Geotech. J. 51
401 (12), 1399-1412.
402 Saba, S., Cui, Y. J., Barnichon, J. D., and Tang, A. M., 2016. Infiltration Column for Studying
403 the Lateral Swell Behavior of Expansive Clay. Geotech. Test. J. 39 (3), 407-414.
404 Sun DA, Cui HB, Sun WJ. Swelling of compacted sand-bentonite mixtures, Applied Clay
405 Science, 2009, 43(3): 485-492.
406 Villar, M. V., García-Siñeriz, J. L., Bárcena, I., & Lloret, A., 2005. State of the bentonite
407 barrier after five years operation of an in situ test simulating a high level radioactive
408 waste repository. Eng. Geol. 80 (3), 175-198.
409 Villar, M. V., and Lloret, A., 2008. Influence of dry density and water content on the swelling
410 of a compacted bentonite. Appl. Clay Sci. 39 (1), 38-49.
411 Wang, J., 2010. High-level radioactive waste disposal in China: update 2010. J. Rock Mech.
412 Geotech. Eng. 2 (1), 1-11.
413 Wang, Q., Tang, A. M., Cui, Y. J., Delage, P., and Gatmiri, B., 2012. Experimental study on
414 the swelling behaviour of bentonite/claystone mixture. Eng. Geol. 124, 59-66.
415 Wang, Q., Cui, Y. J., Tang, A. M., Barnichon, J. D., Saba, S., and Ye, W. M., 2013a. Hydraulic
416 conductivity and microstructure changes of compacted bentonite/sand mixture during
417 hydration. Eng. Geol. 164, 67-76.
418 Wang, Q., Tang, A. M., Cui, Y. J., Barnichon, J. D., and Ye, W. M., 2013b. A comparative
419 study on the hydro-mechanical behavior of compacted bentonite/sand plug based on

420 laboratory and field infiltration tests. Eng. Geol. 162, 79-87.
421 Wang, Q., Tang, A. M., Cui, Y. J., Delage, P., Barnichon, J. D., and Ye, W. M., 2013c. The
422 effects of technological voids on the hydro-mechanical behaviour of compacted
423 bentonite–sand mixture. Soils Found. 53 (2), 232-245.
424 Wang, Q., Cui, Y. J., Tang, A. M., Li, X. L., and Y, W. M., 2014. Time-and density-dependent
425 microstructure features of compacted bentonite. Soils Found. 54 (4), 657-666.
426 Ye, W. M., Zhu, J. Y., Chen, B., Cui, Y. J., and Wang, J., 2012. A device designed for
427 simulating HM behavior of compacted GMZ01 bentonite. KSCE Journal of Civil
428 Engineering. 16 (7), 1178-1184.

Lists of Figures and Tables

(a)

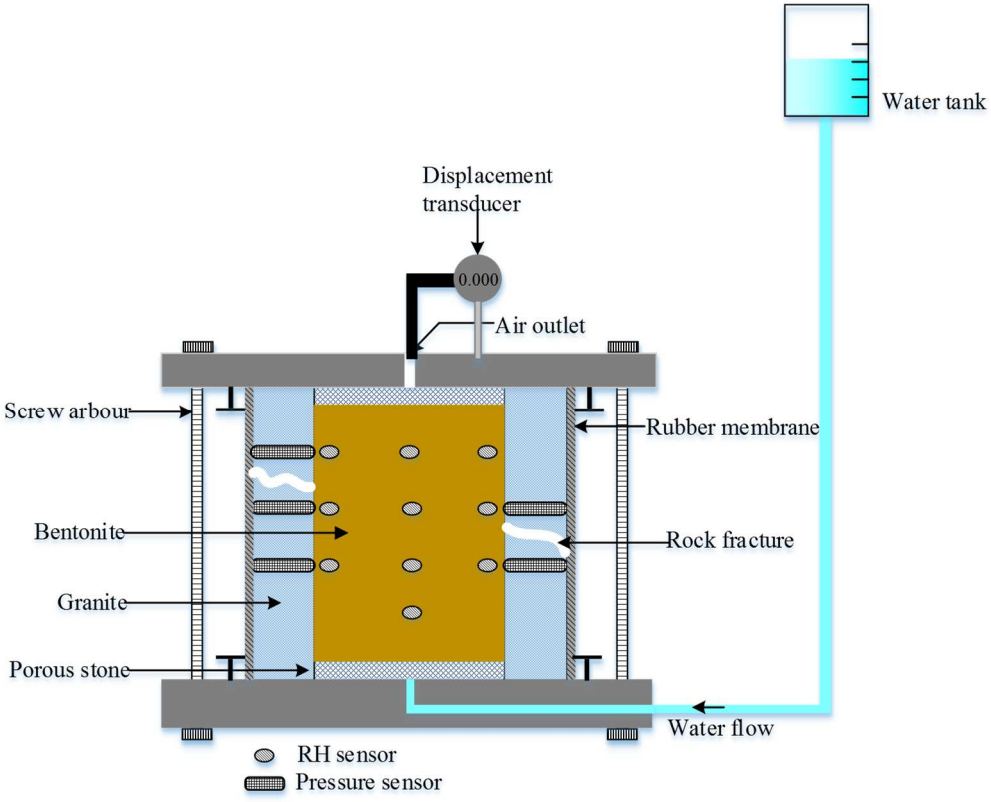

(b)

Fig. 1 Experimental setup, (a) photo, (b) schematic layout

(a) (b)

Fig. 2 Beishan Granite samples, (a) separated samples, (b) assembled sample

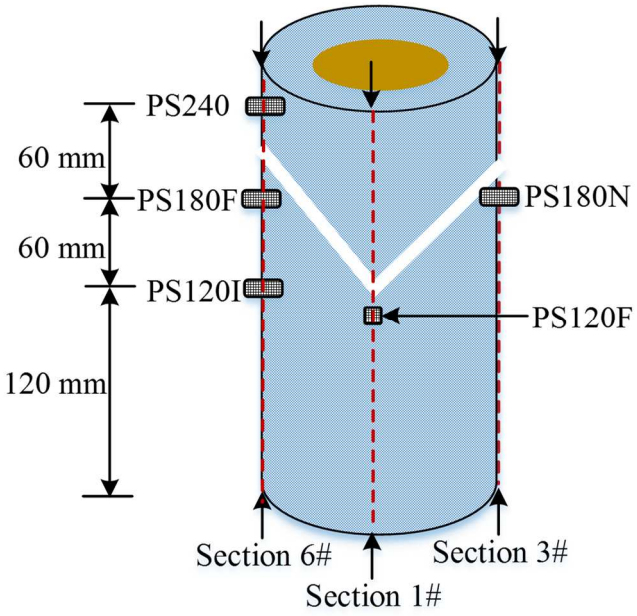

(a) Locations of pressure sensors

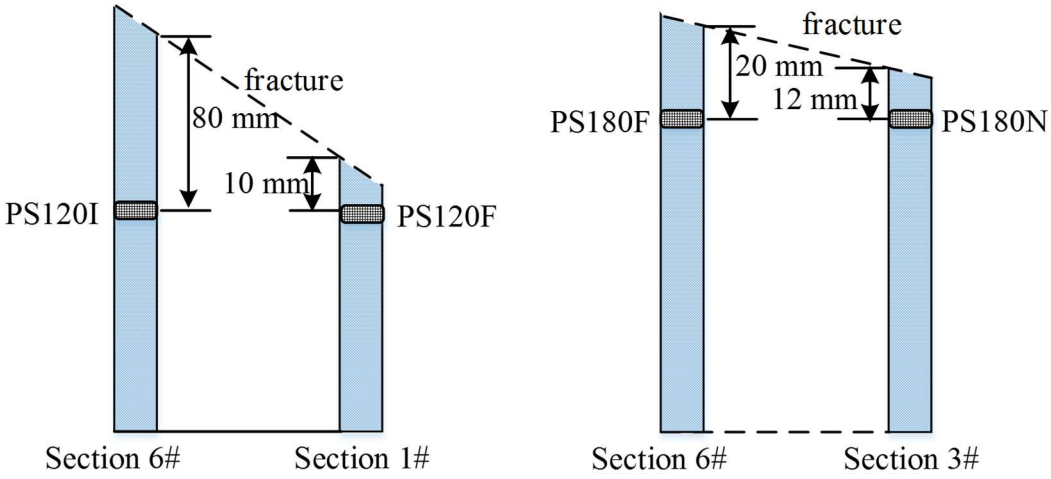

(b) Relative distances of pressure sensors to the fracture

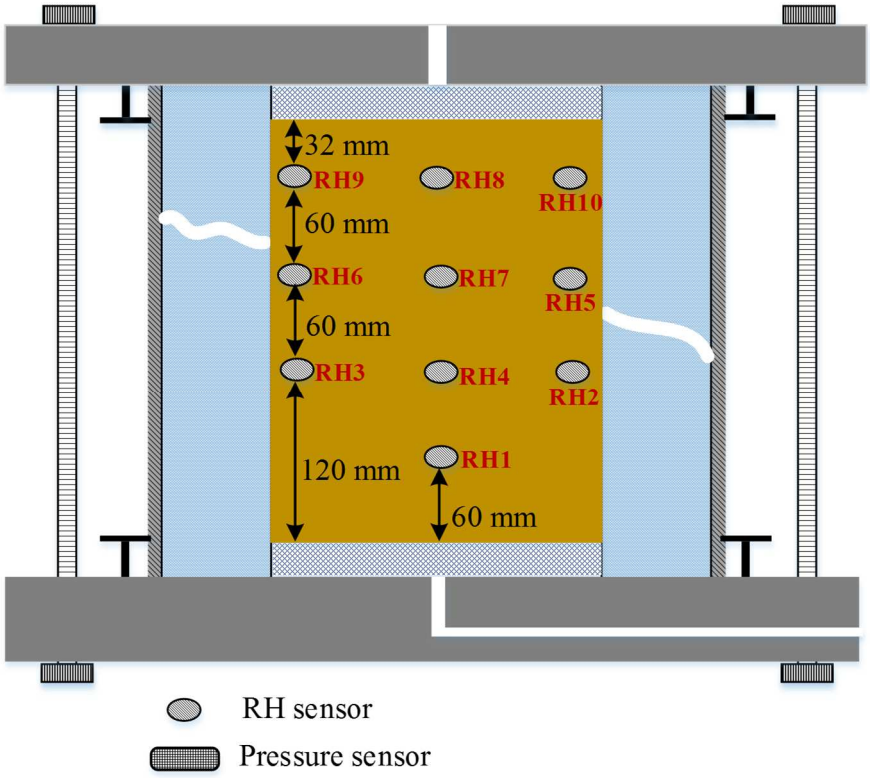

(c) Location of RH sensors

Fig. 3 Positions of different sensors

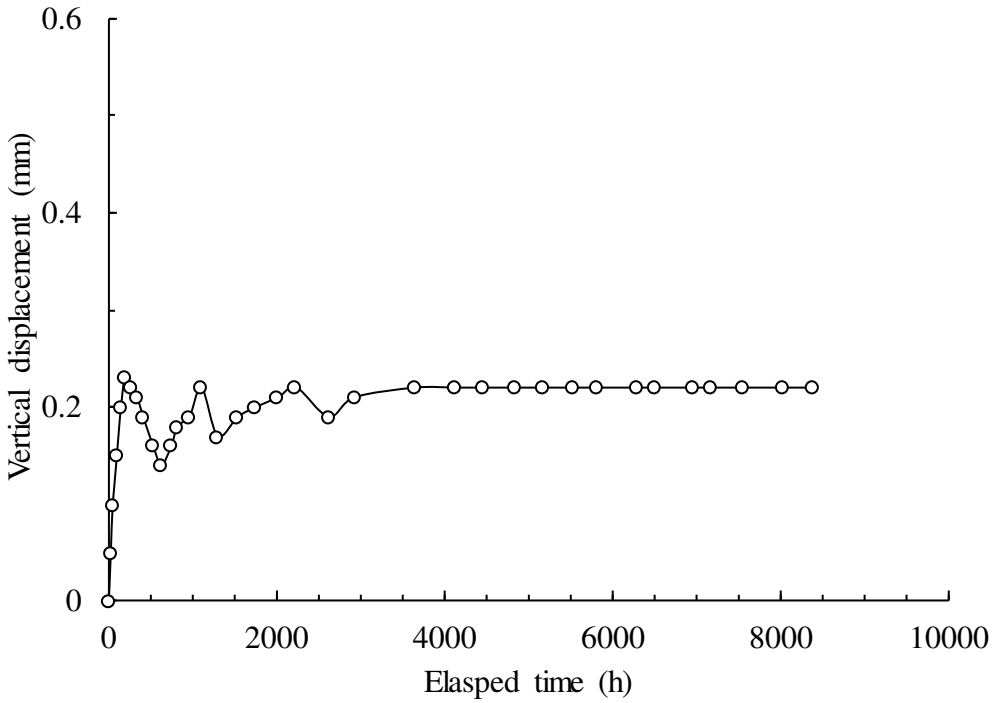

Fig. 4 Vertical displacement of the top plate

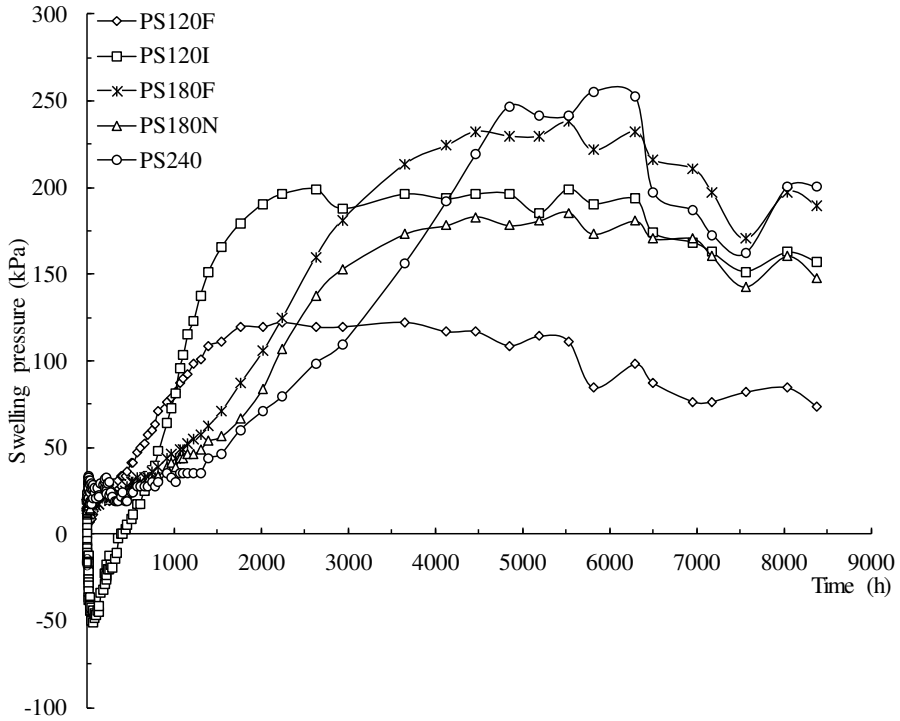

(a)

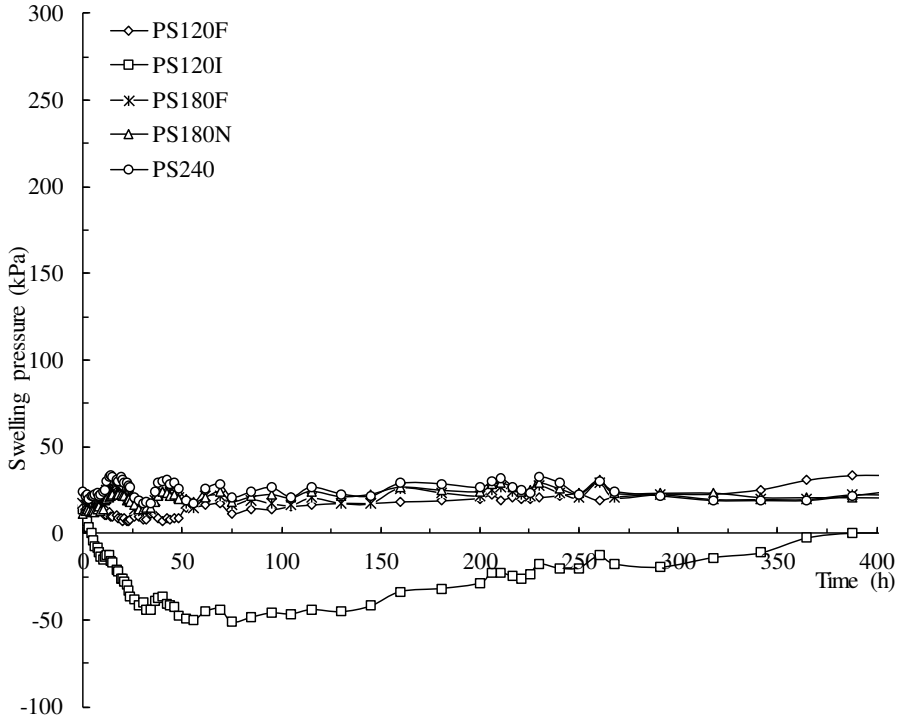

(b)

Fig. 5 Evolution of swelling pressure over time, (a) swelling pressure, (b) swelling pressure in the first 400 hours

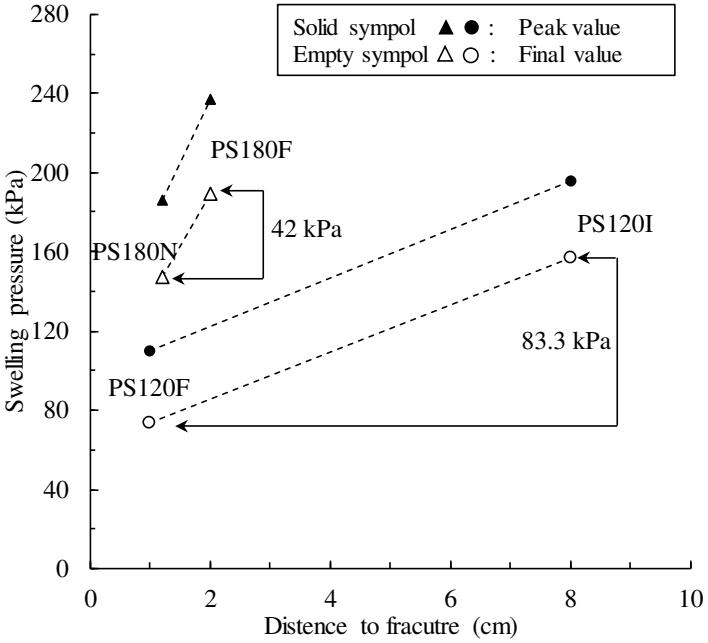

Fig. 6 Relationship between peak and final swelling pressure and distance to fracture

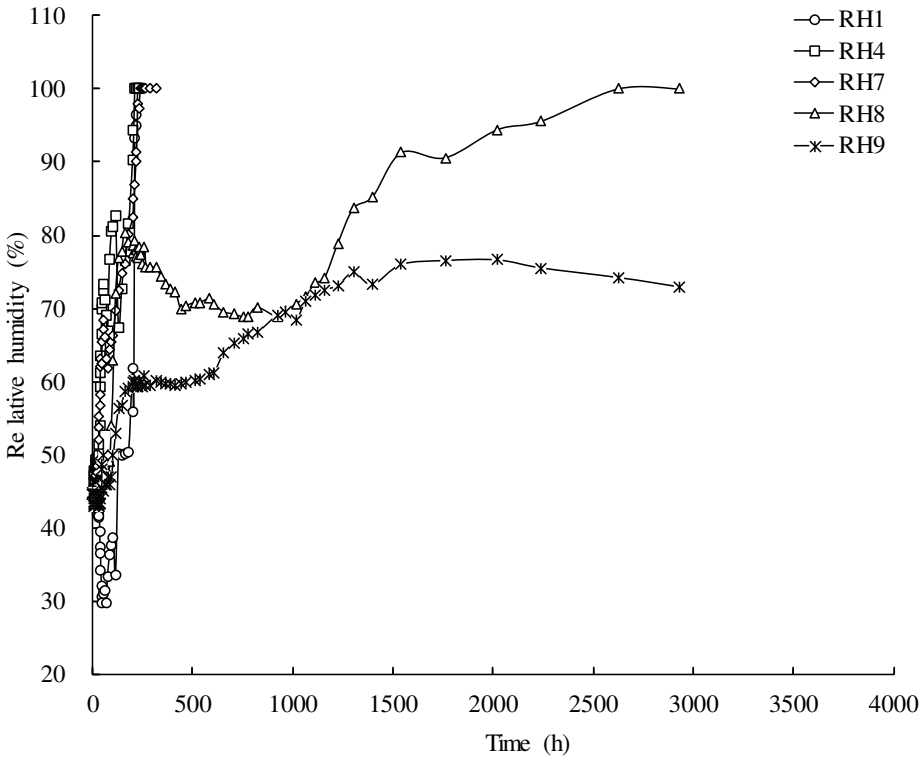
RH1
RH4
RH7
RH8
RH9
Re lative humidity (%)
Time (h)
110
100
90
80
70
60
50
40
30
20
0
500
1000
1500
2000
2500
3000
3500
4000

(a)

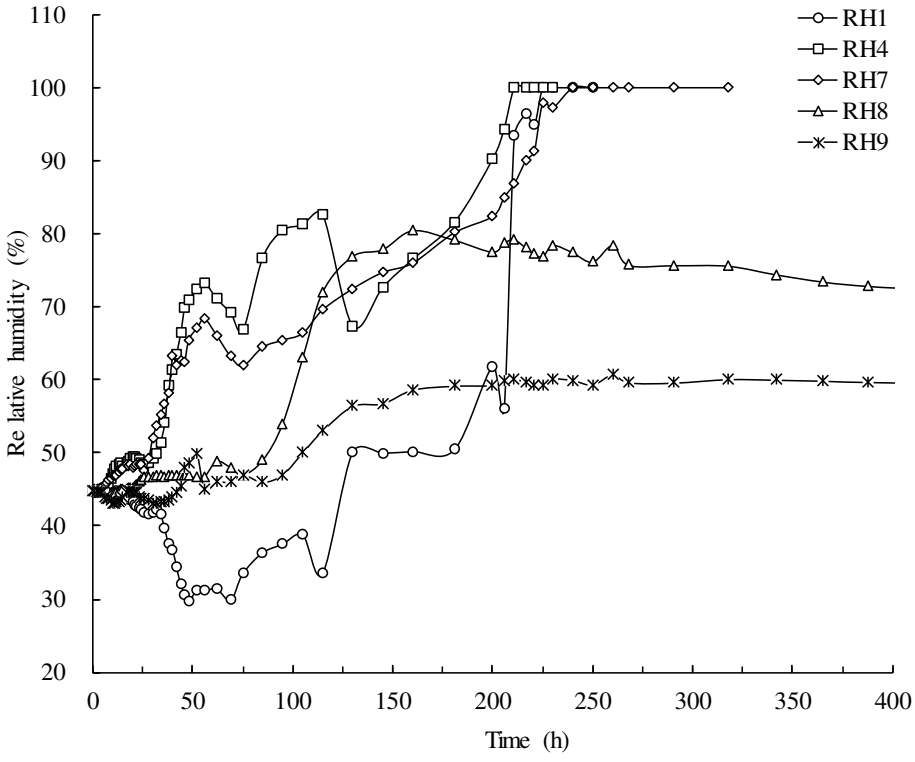
RH1
RH4
RH7
RH8
RH9
Re lative humidity (%)
Time (h)
110
100
90
80
70
60
50
40
30
20
0
50
100
150
200
250
300
350
400

(b)

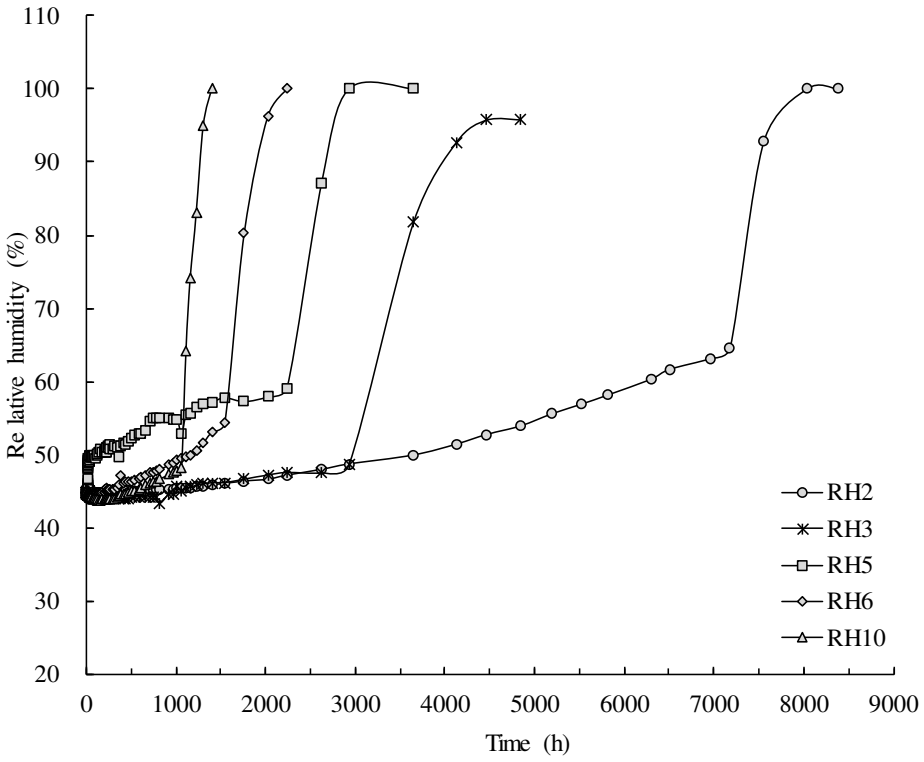

(c)

Fig. 7 Evolution of relative humidity during water infiltration, (a) recordings from sensors RH1, RH4, RH7, RH8 and RH9, (b) recordings from senor RH1, RH4, RH7, RH8 and RH9 in the first 400 hours, (c) recordings from senor RH2, RH3, RH5, RH6 and RH10

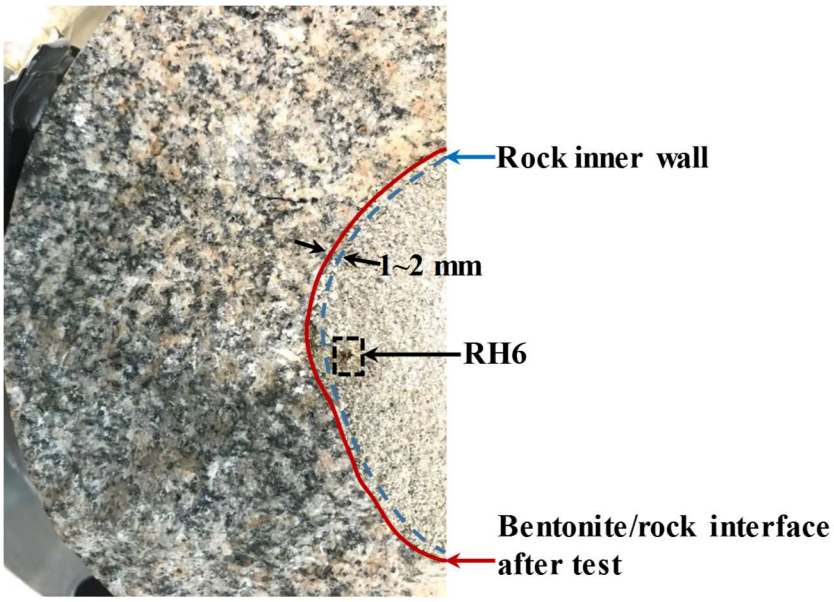

Fig. 8 Intrusion of bentonite into the fracture

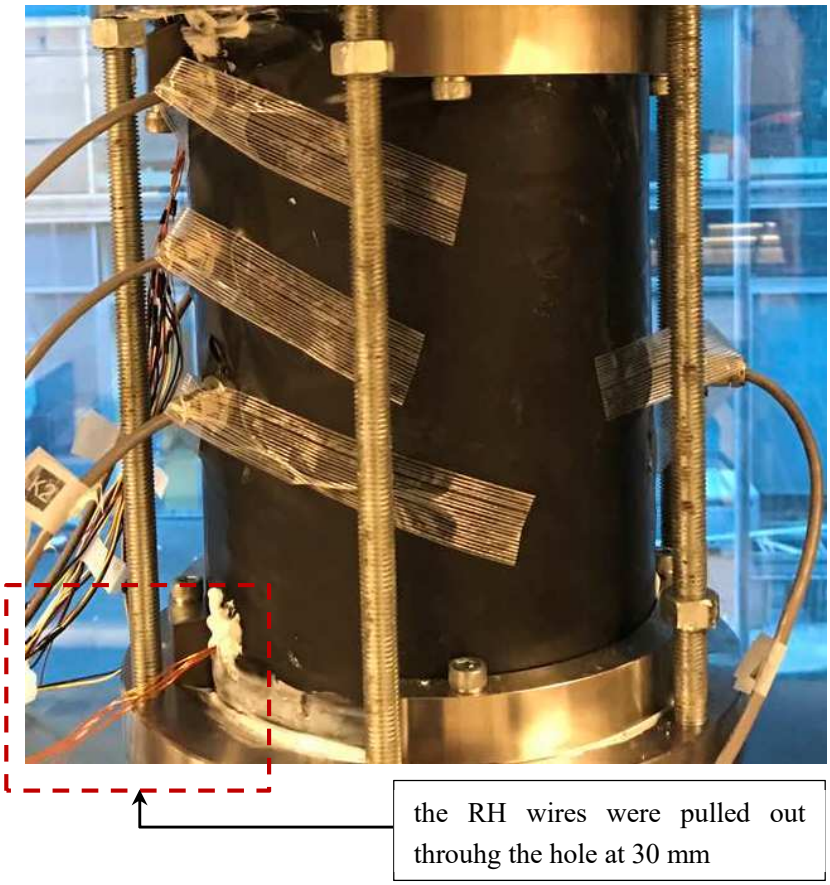

Fig. 9 Detail of RH wires at the hole of 30 mm

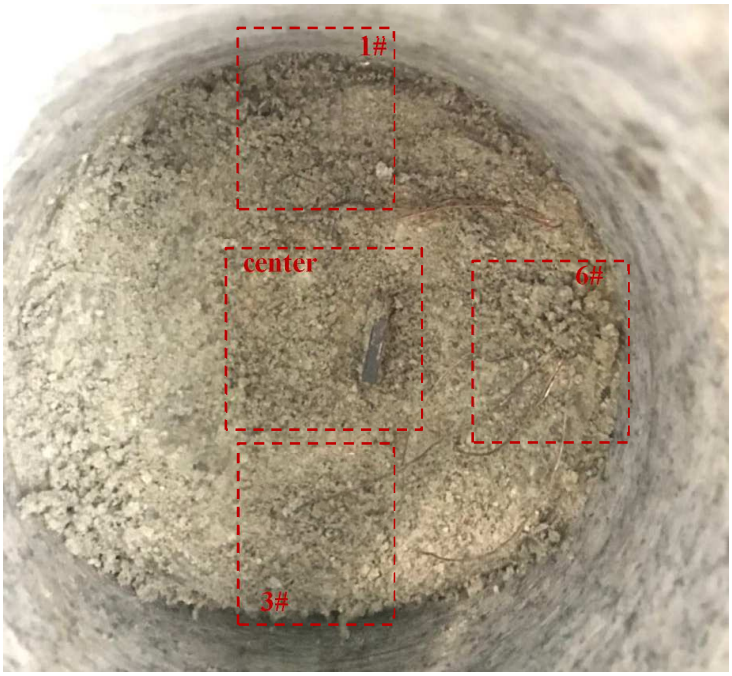

Fig. 10 After-infiltration sample at 60 mm

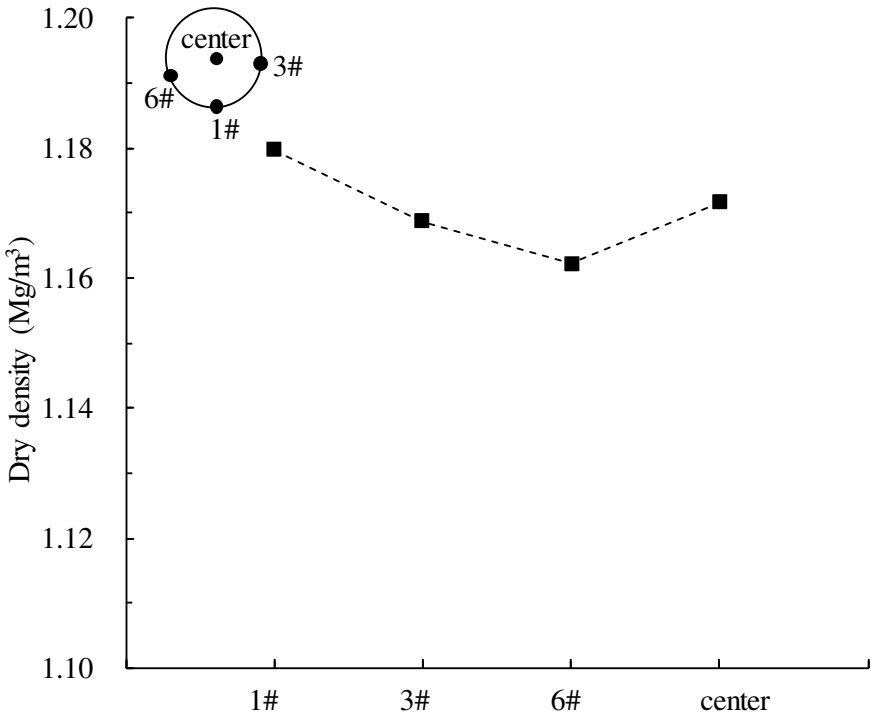

Fig. 11 Variation of dry density of after-infiltration sample at 60 mm

Table 1. Compaction procedure and sample density

Layer	Soil weight: g	Height after compaction: mm	Average diameter: mm	Dry density ρ_d: Mg/m^3
1	141.37	20.0	82.5	1.32
2	140.57	19.9	82.5	1.32
3	141.90	20.1	82.5	1.32
4	141.29	20.0	82.5	1.32
5	142.19	20.1	82.5	1.32
6	141.11	20.0	82.5	1.32
7	141.07	19.9	82.5	1.33
8	141.45	19.9	82.5	1.33
9	141.06	20.0	82.5	1.32
10	141.91	20.1	82.5	1.32
11	142.22	20.0	82.5	1.33
12	141.50	20.1	82.5	1.32
13	224.09	32.1	82.5	1.31
Total	1921.73	272.2	82.5	1.32